UCRL-JC-118707
PREPRINT

Multi-Angle Technique for Measurement of Ground Source Emission

John R. Henderson

This paper was prepared for submittal to the
Society of Photo-Optical Instrumentation Engineers
Orlando, FL
April 17-21, 1995

April 1995

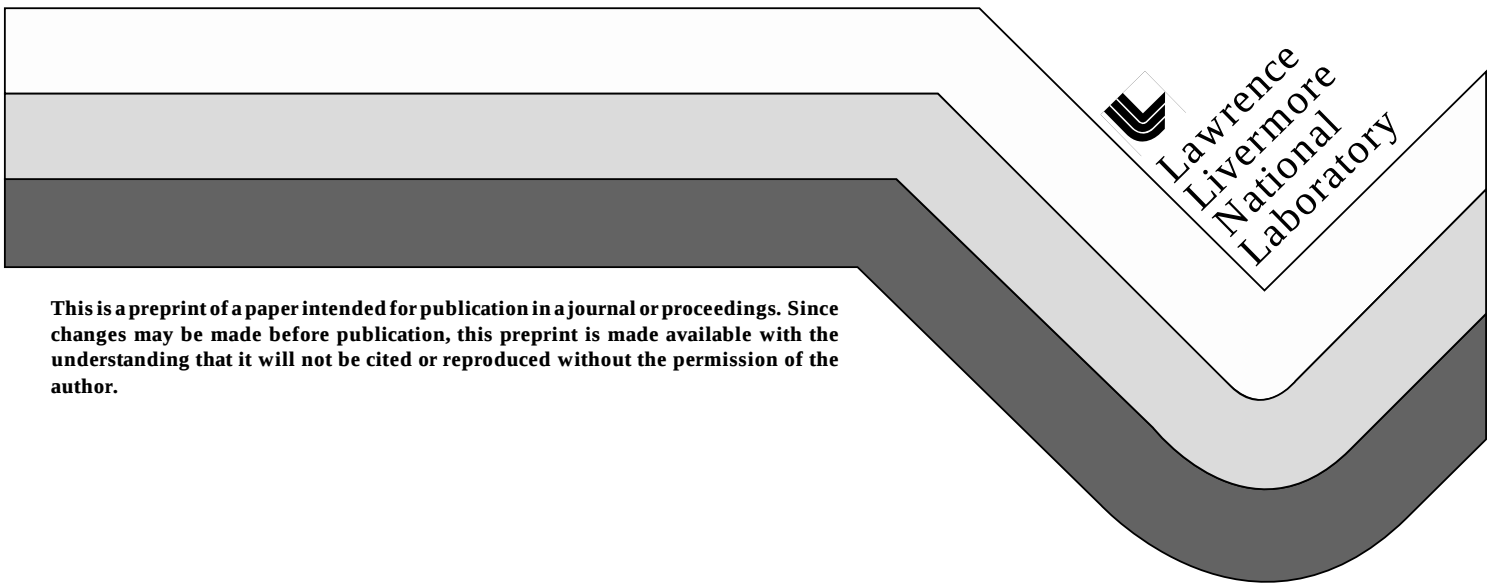

Multi-angle technique for measurement of ground source emission

John R. Henderson

Physics and Space Technology, MS L-043
Lawrence Livermore National Laboratory
Livermore, California 94550

ABSTRACT

TAISIR, the Temperature and Imaging System InfraRed, is a nominally satellite based platform for remote sensing of the earth. One of its design features is to acquire atmospheric data simultaneous with ground data, resulting in minimal dependence on external atmospheric models for data correction. One technique we employ to acquire atmospheric data is a true multi-angle data acquisition technique. Previous techniques have used only two angles. Here we demonstrate the advantage of using a large number of viewing angles to overconstrain the inversion problem for critical atmospheric and source parameters. For reasonable data acquisition scenarios, simulations show source temperature errors of less than 1K should be possible. Tradeoffs between flight geometry, number of look angles, and system signal-to-noise are given for typical parameter ranges.

Keywords: thermometry, infrared, imaging, atmospheric modeling, multi-angle, atmospheric transmission

1. INTRODUCTION

The goal of the Temperature and Imaging System InfraRed (TAISIR) project is to measure ground temperatures in a robust manner, that is, to retrieve ground temperatures even under conditions of poor seeing and with little or no model dependence. The basic TAISIR concept is to use a low spectral resolution imager with a co-aligned high resolution spectrometer. The spectrometer provides atmospheric information needed to correct the imager data for atmospheric attenuation and emission.

Historically, radiosonde or weather satellite information has been used to obtain the atmospheric properties through modeling codes. The accuracy of ground source emission determination has been limited to a few degrees by: the accuracy with which the modeling codes correctly describe the atmosphere; use of non-ideal weather data due to lack of concurrent and / or co-spatial information; and high sensitivity to the presence of aerosols such as due to volcanic eruptions or sub-visual cirrus cloud. Here we will describe a new technique and show how it overcomes all of these problems. The final problem of converting source emission to source temperature through the determination of source emissivity will be addressed in subsequent work.

Background on techniques to measure source emission in a model-independent (or weakly dependent) manner is given in section 2. In our previous work[1] on the multi-angle technique, we presented a new model to more accurately describe the band-averaged transmission. That work is described in section 3. In section 4, the formalism for extrapolating the measured emission as a function of atmospheric column depth to source emission is developed. In section 5, that formalism is used to explore the tradeoffs between number of angles measured, signal-to-noise, and data collection geometry. In section 6, additional factors needed for general applicability of the technique are discussed. The major conclusions and directions for future work are summarized in section 7.

2. BACKGROUND

A number of techniques have been developed to either measure or correct for the effects of atmospheric attenuation and emission. The limitations of conventional techniques have been briefly mentioned above and will not be further discussed. One of the most accurate methods to determine source emission is to view the source from a variety of altitudes. One then obtains a curve of measured emission versus altitude. The data can be extrapolated to zero altitude using a family of curves determined from calibrated measurements or atmospheric modeling, such as with MODTRAN. This technique has been demonstrated to have an accuracy of ≤ 1 K by Byrnes and Schott[2]. Systematic errors will appear with this technique if the source temperature changes during the measurements, e.g. by solar heating. Random ordering of flight altitude solves the problem of detecting the systematic error, but makes the possibility of changes in the source emission or atmospheric conditions more likely due to the longer time to fly the data acquisition profile. The accuracy of this technique depends on the ability to sample the atmosphere in the first few thousand feet above the source. This is the region where most of the attenuation and emission occur. At higher altitudes, there is much less leverage to extrapolate to the ground level source emission and the accuracy suffers. The multi-altitude technique is not appropriate for satellites, high-altitude balloons, or other platforms not capable of flying low altitudes above the source.

Techniques using multiple (specifically two) viewing angles to enhance remote measurements were proposed[3] at least as early as 1967. The multi-angle technique exploits the variation of the transmission and the emission of the atmosphere with the variation of the depth of the atmospheric column. As the viewing angle deviates from the nadir, the column depth increases, the atmospheric emission increases, and the flux seen at a remote sensor decreases for a ground source warmer than the atmosphere. A wide range of accuracies are reported using the technique: Chedin *et al* [4] obtain rms deviations of 1K to 2K simulating satellite observations of sea surfaces, Macleod[5] obtained 0.3K for an airborne platform, and Byrnes and Schott[2] measured rms errors of 1.0K to 6.6K at altitudes of 1000 feet to 6000 feet, respectively. Simulations by Cogan[6] support the magnitude and linear scaling with altitude observed.

The two-angle techniques mentioned above all use a band averaged transmission which creates a systematic underestimate of the transmission off-nadir. More generally, for a given waveband there are three parameters that determine the measured emission: the source emission, the atmospheric transmission, and the atmospheric emission. Equivalently, one can use an effective atmospheric temperature and emissivity (determined from the transmission). The fundamental difficulty with two-angle techniques is that the problem is underconstrained. A minimum of three measurements are needed to solve for this simple model of atmospheric effects, but only two measurements are made. For low altitudes, the atmospheric emission is comparatively small. Two angles techniques either ignore the atmospheric emission, or assume a reasonable atmospheric temperature and emissivity. The errors from the latter are typically small. For high altitude platforms or conditions of poor visibility, the atmospheric emission must be treated accurately, and two-angle techniques are inadequate.

The constraints on measurements from high altitude platforms, inability to directly probe the critical near-surface atmosphere and necessity of an accurate determination of atmospheric emission, mean that previous techniques will be of limited utility. The multi-angle technique allows both constraints to be met. The ability to vary the atmospheric column depth in a known manner permits the separation of atmospheric and source contributions from the measured emission. Additionally, the development of a new model for the variation of the band-averaged transmission with column depth is critical to obtaining accurate results with the multi-angle technique.

3. MULTIPLE ANGLE TECHNIQUES

3.1 Simple model of band-averaged transmission

The measured signal at a remote detector is

$$L_d = \tau * L_s + L_a \,, \tag{2}$$

where L_d is the measured emission, τ is the atmospheric transmission, L_s is the source emission, and L_a is the atmospheric emission. In general, all of these quantities are a function of waveband and viewing angle.

The standard development of multi-angle techniques uses a band-averaged transmission, τ. Taking θ to be the angle from nadir, the transmission as a function of angle is given by

$$\tau = \tau_o^{1/\cos\theta} = \tau_o^{\sec\theta} = \tau_o^{l}, \tag{6}$$

where τ_o is the transmission at nadir and l is the relative depth of the atmosphere. For a non-reflective material (the atmosphere) the emissivity and transmissivity are related by

$$\tau = 1 - \varepsilon \,. \tag{7}$$

The atmospheric emission, L_a, is given by

$$L_a = \varepsilon_a * B_\nu(T_a, \lambda_1,\lambda_2)\,, \tag{8}$$

where $B_\nu(T_a, \lambda_1,\lambda_2)$ is the black body emission for a source at temperature T_a over the waveband from λ_1 to λ_2. Hereafter, the explicit wavelength dependence will be suppressed and we will use the shorthand $B_a = B_\nu(T_a, \lambda_1,\lambda_2)$, and $B_s = B_\nu(T_s, \lambda_1,\lambda_2)$ for the atmosphere and source black body emission.

The source is assumed to have an emissivity ε_s, specular reflectivity R_s, and diffuse reflectivity R_d, which are related by

$$1 = \varepsilon_s + R_s + R_d\,. \tag{9}$$

The source emission is then,

$$L_s = \varepsilon_s*B_s + R_d*\boldsymbol{\varepsilon_A}*B_a + R_s*\varepsilon_a*B_a\,, \tag{10}$$

where $\boldsymbol{\varepsilon_A}$ is the angular average of the sky emissivity, and it has been assumed that the downwelled sky emission is equal to the upwelled sky emission. $\boldsymbol{\varepsilon_A}$ is a function of τ_o and the scene geometry. Combining equations 2, 6, 7, 8 and 10, we have the expression for the detected flux, L_d, as a function of relative atmospheric depth

$$\begin{aligned} L_d(l) &= (1-\tau_o^{\,l})*B_a + (\tau_o^{\,l})*[\,\varepsilon_s*B_s + R_d*\boldsymbol{\varepsilon_A}*B_a + R_s*(1-\tau_o^{\,l})*B_a\,]\,, \\ &= B_a + [\,\varepsilon_s*B_s + R_d*\boldsymbol{\varepsilon_A}*B_a + R_s*B_a - B_a\,]*\tau_o^{\,l} - R_s*B_a*\tau_o^{\,2l}\,, \\ &= B_a * (1 + \beta*\tau_o^{\,l} - R_s*\tau_o^{\,2l}), \end{aligned} \tag{11}$$

where

$$\beta = \varepsilon_s*B_s/B_a - 1 + R_d*\boldsymbol{\varepsilon_A} + R_s\,. \tag{12}$$

The source emission is now given by, using equations 7, 10, and 12,

$$L_s = B_a*(\,\beta + 1 - R_s*\tau_o^{\,l}\,)\,. \tag{13}$$

Note that the source emission is a function of viewing angle (explicitly the column depth) due to the non-zero specular reflectivity. Since there are four fit parameters, B_a, β, R_s, and τ_o, a minimum of four measurements are necessary to determine the source emission. If the specular reflectivity is known or assumed to be zero, we have the previously discussed case where three measurements are needed to determine the source emission.

Here, there are seven parameters of interest, B_s, ε_s, R_d, R_s, B_a, ε_A, and τ_o. The four fit parameters, Equation 9, and the relation between ε_A and τ_o leave the problem underconstrained for any single waveband. Since T_s is independent of wavelength, T_a nearly so (depending on the average optical depth in the band), and there are generally some constraints on the ground properties, such as slow variation of ε_s with wavelength, the problem is likely to be constrained for multiple wavebands.

3.2 First order model for transmission

The shortcoming of the naive model is that Equation 6 is not a realistic description of how the band-averaged transmission varies with relative atmospheric depth. Various empirical relations[7] have been used to account for the observation that the naive model of transmission underestimates the transmission off-nadir.

The insight exploited here is that there is line structure within the waveband. Figure 1 shows a generic transmission spectrum for within a waveband of observation. Physically, the significant fraction of the band with high transmission will still have high transmission for multiple atmospheric depths. The opaque regions will remain opaque. The only regions to have significantly lower transmission with increasing atmospheric depth are the regions on the edge of the absorption lines. Since only a small fraction of the band has its transmission lowered, the overall band transmission is higher than one would estimate using only the band averaged transmission.

The problem is how to succinctly include this important information about band structure into the formalism used to determine the source emission. Figure 2 shows a histogram of the data in Figure 1, where the transmission values have been plotted as a decreasing function of fraction along the waveband. Also shown are the band averaged transmission, a two parameter step function model for the intra-waveband structure, and a three parameter model for the structure. The three parameter model is described in more detail in Reference 1. It is shown here to illustrate that there are succinct models for the waveband structure that can be used if needed. The rest of this paper will focus on the two parameter, “first order,” model since it appears to be sufficiently accurate for the problem at hand and has less mathematical complexity than the three parameter model.

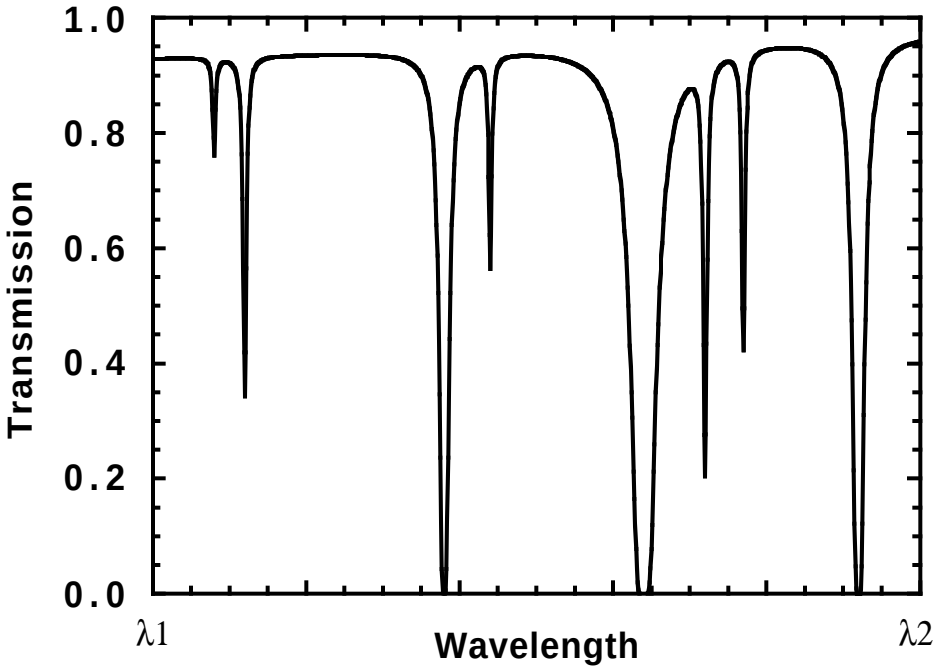

Figure 1. Illustration of the variation of transmission with wavelength within the waveband to be used for a measurement.

The first order model is a two parameter model that divides the band into a transmissive and an opaque region. The parameters are the transmissive fraction of the band, f_1, and its transmission, τ_1. The opaque portion has a transmission of zero and accounts for a fraction $(1 - f_1)$ of the band. The depth-dependent transmission, $\tau(l)$, is now given by

$$\tau(l) = f_1 * (\tau_1^{l}), \tag{14}$$

and the atmospheric emission is given by

$$L_a = f_1*(1 - \tau_1^{l})*B_a + (1 - f_1)*B_o, \tag{15}$$

where B_o is the emission for a black body at the temperature, T_o, of the opaque layer. (By definition, the opaque layer has an emissivity on one.) Comparing to the previous section, we find that

$$f_1*\tau_1 = \tau_o . \tag{16}$$

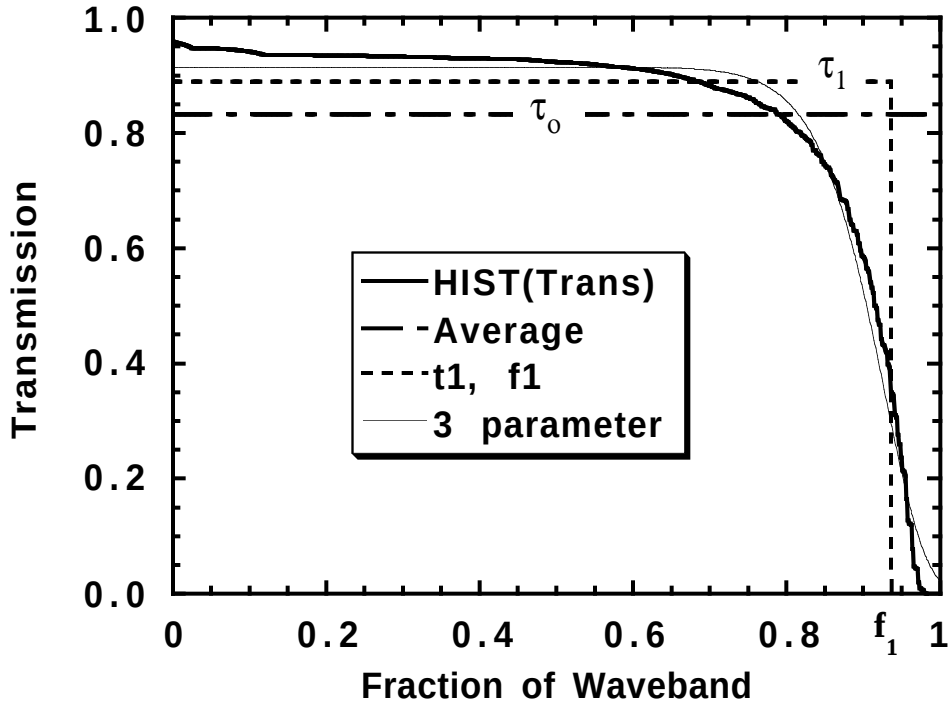

Figure 2. Histogram of the data in Figure 1, along with several model descriptions of the structure of the histogram. The average of the transmission is the single parameter model typically used, the two and three parameter models are described in the text.

For two atmospheric depths, the transmission is, noting that $f_1 < 1$,

$$f_1 * \tau_1^2 = \tau_o^2 / f_1 > \tau_o^2 ,$$

demonstrating the underestimate of the transmission resulting from use of the band averaged transmission, τ_o.

The flux seen at a detector can be derived as in the previous section. The result is

$$L_d(l) = A + B * \tau_1^l + C * \tau_1^{2l} , \tag{17}$$

where

$$A = f_1 * B_a + (1 - f_1) * B_o , \tag{18}$$

$$B = \varepsilon_s * B_s + R_d * \varepsilon_A * B_a + R_s * (1 - f_1) * B_o + R_s * f_1 * B_a - B_a , \tag{19}$$

$$C = - f_1^2 * R_s * B_a . \tag{20}$$

Since we have the same number of constraints as before, but have added a wavelength dependent parameter f_1 and a nominally wavelength-independent parameter T_o (giving $B_o(\lambda)$), the problem is underdetermined. Since f_1 depends primarily on the fraction of strong lines in the waveband, and secondarily on their strength, one would expect f_1 to have only a weak dependence on the precise amount of the absorbing agent. Previous modeling[1] shows that this is the case. Atmospheric modeling codes or spectroscopic measurement of water content are sufficiently accurate to determine f_1.

4. MEASUREMENT OF SOURCE EMISSION

For simplicity, we will assume that the specular reflectivity of the source is zero. Equations 17 to 20 become

$$L_d(l) = A + B*\tau_1^{\,l} \quad , \tag{21}$$

where

$$A = f_1*B_a + (1 - f_1)*B_o \quad , \tag{22}$$

$$B = \varepsilon_s*B_s + R_d*\varepsilon_{\mathbf{A}}*B_a - B_a \quad . \tag{23}$$

The source emission is nominally the value of the detected emission when $l = 0$. This is

$$L_d(l = 0) = A + B \tag{24a}$$

$$= \varepsilon_s*B_s + R_d*\varepsilon_{\mathbf{A}}*B_a - (1 - f_1)*(B_a - B_o) \quad . \tag{24b}$$

The first two terms are just the expected result from equation 10. The last term is independent of the source itself, and is due to the fact that there is no way to "see through" the opaque regions. Since B_o and f_1 can be modeled well, and B_a can be determined from equation 22, the errors in the third term should be small for the regions of interest. It is thus possible to determine the source emission.

Previous measurements using the two-angle technique[2] show errors that increase with altitude. This is to be expected since the opaque region correction becomes more important as altitude increases and the air temperature is cooler.

5. OPERATIONAL REQUIREMENTS ON MEASUREMENT ACCURACY

The basic behavior can be illustrated by considering a simplification of equation 21. Letting

$$\tau_1 = (1 - \delta) \tag{25}$$

equation 21 becomes

$$L_d(l) = A + B*(1-\delta)^l \quad (26a)$$

$$\approx (A + B) - B*l*\delta \ , \quad (26b)$$

where the source emission is still given by (A + B). This is a straightforward problem of linear least squares analysis. The error in determination of the source emission is then limited by the number of points and the accuracy of each measurement in a straightforward manner. In the general (non-linearized) case, the determination of source emission will be more uncertain due to the extra fit parameters. Essentially, the uncertainty in the curvature (neglected in Equation 26b) adds uncertainty to emission measurement.

The general scaling of measurement error with number of looks, N, with maximum atmospheric depth (taking closest approach to be one), l_{max}, and for system noise equivalent temperature difference, NETD, was obtained for the linear approximation. For a 300K source, mid-latitude conditions, and "typical" conditions in the 10 micron transmission window, a synthetic data set was generated for given N, l_{max}, and system NETD. For each set of conditions, a "measurement" with noise (from the NETD) of the radiance as a function of atmospheric depth was generated. The specific depth values were determined for a constant velocity flyover. The source emission and its error was determined from a linear least squares fit. This was repeated 40 times to do statistical analysis of the fitting procedure. The error values from the least squares and statistical analyses typically agreed to better than 10%. The error scaled linearly with NETD. For l_{max} = 2.5 and NETD = 1.0 K, the emission error (expressed as equivalent temperature) as a function of N was

$$\sigma_{Ts} \approx 3.489 \ / \ \sqrt{N} \ . \quad (25)$$

For N = 15 and NETD = 1.0 K, the emission error as a function of l_{max} was found to be

$$\sigma_{Ts} \approx 0.369 * [1 + 2/(l_{max} - 1)] \ . \quad (26)$$

These relations give only the approximate scaling relations due to the expedient of linearizing the fit.

To determine the measurement accuracy for the full functional form, sample data for N = 15, l_{max}= 2.5 were run for the range of atmospheric conditions likely to be found and for several values of NETD. Some of the results are shown in Table 1. In general, the uncertainty is proportional to NETD. However, for NETD > 1.0, the inversion becomes difficult and the values for the fit parameters often are not physically reasonable (e.g. $\tau_1 > 1$). This can be used as a qualitative measure of the goodness of the fit. The lowest errors are obtained for Ts = 278K. This is because the source and effective atmospheric temperatures are the same. In this situation, the atmosphere could be completely opaque, and one would still obtain the correct

source temperature. For warmer source temperatures, the rms errors are higher, particularly where the transmission is low. Note that the lowest transmission ($f_1 * \tau_1$ = 0.24) still has a reasonable ability to recover the source temperature.

Table 1. One sigma uncertainty in source emission due to inversion errors. Uncertainty is reported as temperature equivalent at 300 K. The f_1, τ_1 values correspond to: the edge of the transmission window, typical values in the window, and the best values in the window for mid-latitude summer conditions in MODTRAN. Other parameters are: N = 15, l_{max}= 2.5, NETD = 0.2 K.

	Ts = 278K	Ts = 300K	Ts = 320K
f_1, τ_1 = 0.6, 0.4	0.22	1.85	1.84
f_1, τ_1 = 0.95, 0.75	0.18	0.52	0.58
f_1, τ_1 = 1.0, 0.9	0.14	0.64	0.51

6. GENERAL APPLICABILITY OF THE MULTI-ANGLE TECHNIQUE

The discussion above has largely focused on systems where the shortest column depth is a nadir view. This in not a requirement of the technique. In the general case, one sets the shortest column depth in the data set to one and extrapolates to zero depth as before. The penalty for non-nadir viewing is that the geometry typically restricts l_{max} to smaller values. Conditions such as distortion through the atmosphere, limited observation time, or constrained flight path will limit l_{max}.

It is expected that shortcomings of the first order model can be improved by using a higher order model and/or more realistic models for the the atmospheric emission. Recently completed experimental measurements will be used to investigate this.

7. CONCLUSIONS AND FUTURE WORK

The development of a new model for scaling the atmospheric transmission along with a full implementation of the multi-angle technique is a powerful tool for measuring thermal emission under conditions of poor seeing. While the performance is comparable to standard modeling techniques under good visibility, there is relatively little degradation of the measurement capability of the multi-angle technique for conditions of poor seeing. It is critical to have at least four, and preferably ten to twenty viewing angles to properly utilize the technique. The need for a system NETD of about 0.2 K is also more demanding than most current systems.

Conventional modeling techniques are a good technique for determining the atmospheric parameters. In contrast, the multi-angle technique requires unreasonably large signal-to-noise to obtain useful measurements. Mathematically, the parameters in Equation 21 are highly correlated and not well determined in the inversion. Because of the anti-correlation between parameters A and B (see Equation 26b), the source emission is well determined.

Future work needs to look at the benefits of using both standard modeling and the multi-angle technique simultaneously. The effects on including more complex atmospheric structure need to be investigated. Finally, the technique needs to be expanded to determine the source emissivity and atmospheric parameters needed to convert the source emission into a source temperature.

8. ACKNOWLEDGMENTS

Deanne Proctor performed most of the MODTRAN runs and collected the synthetic data into a useful format. This work was performed under the auspices of the U.S. Department of Energy by Lawrence Livermore National Laboratory under contract No. W-7405-Eng-48.

9. REFERENCES

1. J. R. Henderson, "Remote Measurement of ground Temperature and Emissivity," *SPIE Proceedings 2269*, pp. 610-521, July 1994.

2. A. E. Byrnes and J. R. Schott, "Correction of thermal imagery for atmospheric effects using aircraft measurement and atmospheric modeling techniques," *Appl. Opt.*, **25**, pp. 2563 - 2570, August 1986.

3. P. M. Saunders, "Aerial Measurements of Sea Surface Temperature in the Infrared," *J. Geophys. Res.*, **72**, pp. 4109 - 4117, 1967.

4. A. Chedin, N. A. Scott, and A. Berroir, "A Single Channel Double-Viewing Angle Method for Sea Surface Temperature Determination from Coincident METEOSAT and TIROS-N Radiometric Measurements," *J. Appl Meterol.*, **15**, p. 173, 1976.

5. I. D. Macleod, "An Airborne Thermal Remote Sensing Technique," M.S. Thesis, Rochester Institute of Technology, Rochester, NY, 1983.

6. J. L. Cogan, "Passive remote sensing of slant path transmittance," *Appl. Opt.*, **27**, pp 3280-3289, August 1988.

7. R. J. Merickso, "Enhancements to Atmospheric-Correction Techniques for Multiple Thermal Images," M.S. Thesis, Rochester Institute of Technology, Rochester, NY, 1992.

Technical Information Department • **Lawrence Livermore National Laboratory**
University of California • Livermore, California 94551